Extracted from

International Masonry Conference 2026

State of the Art in Masonry Research

Proceedings of the
11th International Masonry Conference (IMC 2026), Lübeck, Germany,
12–15 July 2026

Edited by Birger Gigla, Miklós Molnár and Nigel Shrive

Published by
The International Masonry Society
c/o Lucideon Limited – Stone Business Park, Brooms Road, Stone, Staffs, ST15 0SH

Link to the full conference proceedings

Fraunhofer IRB Verlag

Mechanism Matters: Lessons from Calibrating Continuum FE Models of Calcium-Silicate Masonry

Abide Aşıkoğlu, Michele Longo, Paul A. Korswagen

Abstract: This paper presents insights from numerical simulations of a quasi-static test on a full-scale calcium-silicate brick masonry building representative of Dutch terraced housing. A set of continuum finite-element models was evaluated using different combinations of material parameters, boundary conditions, and modelling strategies, while engaging multiple analysts. Several model configurations achieved good agreement with the experimental response, including stiffness, lateral strength, or damage evolution. However, despite this apparent agreement, the predicted global damage mechanisms could differ from those observed experimentally. The numerical models were dominated by diagonal in-plane cracking, whereas the experiment exhibited global rocking combined with in-plane and out-of-plane failure. By cross-comparing multiple parameter combinations, the study highlights the importance of explicitly verifying damage mechanisms and transparently documenting choices as integral components of mechanism-based calibrations.

Keywords: Damage mechanism, numerical modelling, URM, calibration, epistemic uncertainty.

1 Introduction

In numerical modelling of masonry structures, calibration is often employed as a deterministic approach. Every step in the modelling process, from geometry to boundary conditions to constitutive law, is a layer of assumptions based on engineering judgement or experience. The selection of modelling approach, assumptions and analysis techniques significantly influences numerical predictions [1–4]. Even under similar assumptions, discrepancies persist among modelling strategies which are primarily user-dependent, driven by modelling choices, representation of seismic actions, and interpretation of outcomes. Benchmark analyses highlight substantial epistemic uncertainty, arising from subjective modelling decisions and interpretation, which further complicates reproducibility and reliability. Numerical models of unreinforced masonry (URM) structures are typically validated using global metrics, such as force-displacement response, global

https://doi.org/10.60628/9783738810400-69

stiffness, and peak lateral strength. While these metrics are informative, they do not guarantee accurate reproduction of governing damage mechanisms. Calibration is rarely straightforward, and it is an iterative process, fundamental for identifying influential parameters and ensuring model robustness. Analysts often perform numerous iterations to achieve satisfactory agreement with experimental data, yet published studies usually report only the final model, overlooking the complexity of the process. This lack of transparency can misrepresent calibration as a single-step procedure rather than a systematic trial-and-error approach. The present paper addresses these challenges by evaluating a failure-mechanism-based calibration of a continuum finite element model (FEM) of an existing experimental full-scale calcium-silicate (CS) URM building test under quasi-static loading. Multiple modelling strategies, material parameter combinations, and boundary condition assumptions were explored to assess their influence on global response and damage evolution. By engaging systematic cross-comparison of model variations, the study provides insights into the limitations of calibration based solely on global metrics and demonstrates the importance of verifying damage mechanisms explicitly.

2 Experimental Data

The prototype tested was a full-scale CS brick masonry assemblage, representative of the construction style commonly found as Dutch terraced houses built between 1960 and 1980. These houses usually have two storeys and are constructed from unreinforced masonry. Notable features include the use of cavity walls and substantial façade openings. The inner and outer leaves of the cavity walls are typically joined by steel ties, with CS brick masonry serving as the primary material for the inner load-bearing section. The tested assembly comprises CS brick masonry walls (forming the inner leaf) and concrete floors. The specimen’s design incorporates the typical characteristics of terraced houses, such as slender piers resulting from the large façade openings, and limited connection between the masonry piers and the concrete floor slabs, as seen in Fig. 1a-b.

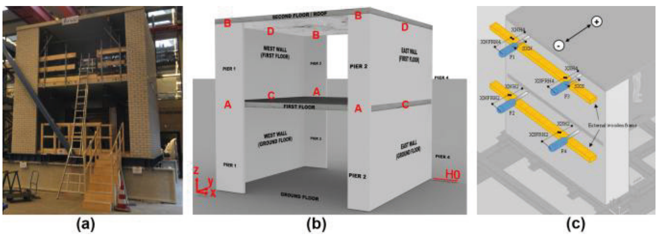

Fig. 1 Experimental configuration, (a) a full-scale test specimen, (b) labelled components, and (c) four actuators as loading instrumentation [5]

The structure incorporates two principal load-bearing walls, situated on the west and east sides of the building (Fig. 1). Each façade was constructed with two piers, one measuring 660 mm in width and the other 1100 mm. The floors consisted of two precast concrete slabs laid across the load-bearing walls, set in place with a mortar bed joint. On the first floor, horizontal anchors measuring 6 mm in diameter were embedded within the floor and built into the piers to secure them (Fig. 2a). For the second floor, the slab was supported by the east and west load-bearing walls (Fig. 2c-d). During construction, however, the slab was initially placed only on the load-bearing walls, and the gap between the pier and slab was later filled with mortar (Fig. 2b). The lateral load was applied using four actuators, arranged to maintain equilibrium such that the combined force from actuators F1 and F3 (second floor) was equal to that from F2 and F4 (first floor, Fig. 1c). The loading sequence consisted of three phases: initial (0-3 mm), pre-peak (3-15 mm), and post-peak (15-85 mm), designed to capture the full range of response from elastic behaviour to failure. Each displacement level was applied three times within each cycle. The crack propagation at each cycle is presented in Fig. 3, which is further discussed in Section 4.

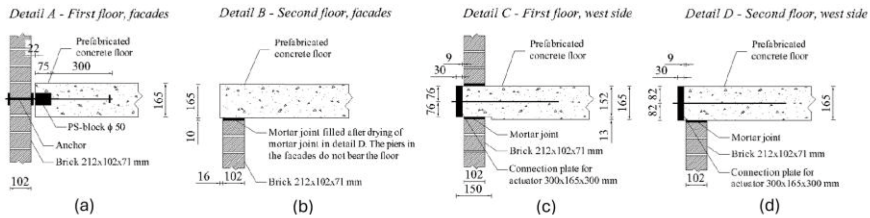

Fig. 2 Construction detail of the connection between concrete floors and walls [5]

3 Numerical Model

The finite element model considers the anisotropy of the masonry resulting from different stiffness in the direction of the bed and head joints through a smeared constitutive law, namely the Engineering Masonry Model (EMM) [6]. The Coulomb friction failure criterion simulates a shear failure mechanism.

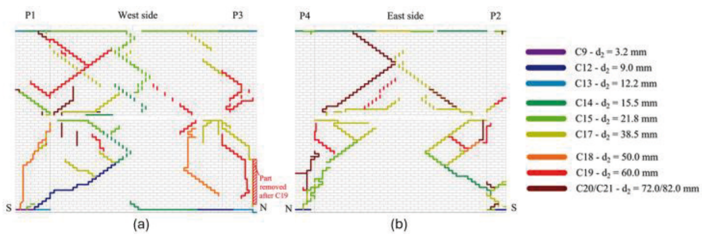

Fig. 3 Cumulative crack distribution: (a) West side, and (b) East side [5]

The tensile properties of the masonry are determined by the tensile strengths of both the head and bed joints. Specifically, the head joint's tensile strength is governed by the frictional shear stress present in the bed joint. For compressive behaviour, the assessment is carried out perpendicular to both the bed and head joints. Eight-node shell elements, CQ40S with bending and membrane actions, were used to model the slab and wall components. CL18B, three-node beam elements, represented actuator-connected beams, while L2TRU, two-node truss elements, linked loading beams to floors (see Fig. 3). Concerning the wall-floor connections shown in Fig. 2, models with fully fixed assumptions are presented in this paper. Two types of analyses were considered, monotonic, and cyclic pushover. The monotonic analysis guided calibration, while the cyclic pushover was performed only after achieving a calibrated response. The load was applied monotonically and incrementally with a uniform load step of 0.25 mm. For cyclic loading, one cycle was applied at each increment using a simplified protocol.

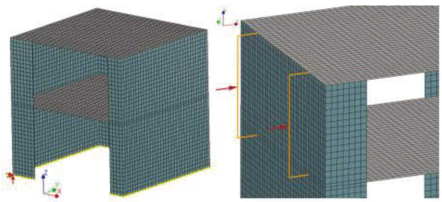

Fig. 4 3D view of the FEM and load application

4 Calibration Process

The calibration framework organised modelling decisions across five layers (Fig. 5), geometry definition; element formulation and discretisation; loading protocol; boundary and interface conditions (wall-floor connections); and material modelling strategies and parametrisation. While multiple pathways exist within this framework, this paper reports material parameter combinations within the EMM approach. Key aspects are shown in colour in Fig. 5; grey elements indicate analysed but unreported modelling variations. The numerical model was initially defined using experimentally obtained material properties for CS masonry [7], thereby establishing a baseline reference model (See V3 in Fig. 7). In-plane piers dominated the simulated damage progression, while out-of-plane walls contributed minimally to the response. Moreover, the model was unable to capture the strength degradation. During calibration of post-peak behaviour, the nonlinear interface properties and their interactions were iteratively assessed; however, cyclic pushover analyses often faced numerical divergence due to the complexity of the interface. To enhance stability and efficiency, interface elements were omitted, and fixed wall-floor connections were assumed in subsequent models.

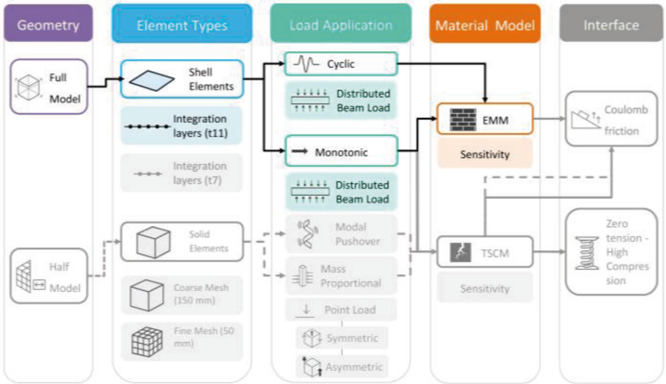

Fig. 5 Calibration framework highlighting the parameters analysed in this paper (coloured)

Within the framework, one path focused on material properties to achieve agreement with the experimental response (Fig. 5). Following baseline comparisons, parameters including Young's modulus, compressive strength, tensile strength, fracture energy (in compression, shear, and tension), and cohesion were iteratively varied one parameter at a time (e.g., V3-V7, Fig. 7) to evaluate first-order effects on global force-displacement response and damage patterns. Although informative, this single-parameter strategy was insufficient. Thus, the calibration subsequently evolved to varying multiple parameters, recognising interdependencies among stiffness, strength, energy dissipation and continuum behaviour in EMM.

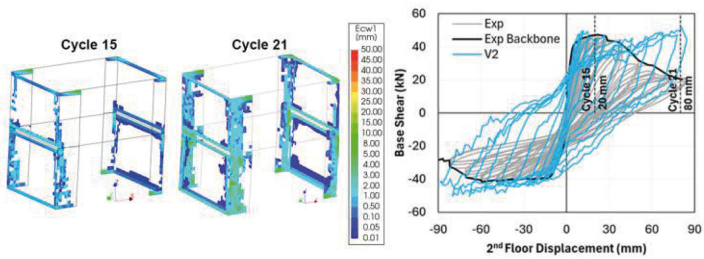

Fig. 6 Model with interface (V2) in terms of crack evolution and hysteretic behaviour

4.1 Model Variations

Fig. 7 illustrates a series of seven scatter plots comparing different material properties across multiple model versions (ranging from 3 to 33). When viewed horizontally, these plots provide an overview of the material combinations considered in the study. Additionally, three EMM head-joint failure modes were considered, direct tensile strength input (DHBJ); diagonal cracking for stair-step failure (Diagonal); and friction-based tensile strength using cohesion and friction angle (HJ-Frict). The first plot shows Young's modulus (E) for two directions: E_x and E_y, respectively parallel and perpendicular to bed joints. In most cases, the experimental values were adopted, except for a few models where higher values were introduced to explore their interaction with low compressive strength and fracture energy. The second plot depicts compressive strength (f_c), fluctuating significantly between 2 and 7 MPa across the model versions. The use of low compressive strength values for CS masonry was based on the observed failure mode (Fig. 3), characterised by brick splitting. This choice is further supported by a previous numerical simulation report on CS masonry [8]. Within this continuum material approach using EMM, accurate modelling of CS masonry requires defining a lower compressive strength to capture its brittle post-peak behaviour. The third plot illustrates fracture energy in compression (G_{fc}), which starts with a high value of 27 N/mm (experimental) and drops significantly for most versions. In practice, f_c must be calibrated in tandem with $G_{fc,}$ as lowering f_c without a reduction in G_{fc} can suppress softening, alter or delay damage localisation. The fourth plot represents tensile strength (f_t) for two orientations: bed joint (f_{tb}) and head joint (f_{th}). Most values cluster around 0.2 MPa, consistent with the experimental data. Although some early versions show zero values for head joint tensile strength, its value is internally computed by the software [6]. Eventually, equal tensile strength values were adopted for both bed and head joints in the later models. These values were set lower than the experimental ones to capture diagonal cracking and overall brittle behaviour. The fifth graph depicts fracture energy in tension (G_{ft}), remaining nearly constant at 0.012 N/mm except for a slight increase in versions 26-30 to enhance energy dissipation in the post-peak response. The sixth graph plots fracture energy in shear (G_{fs}), which mostly remained at 100 N/mm except for a few lower attempts to evaluate its interaction with other reduced parameters. Finally, the seventh plot shows cohesion (c), varying between 0.02 and 0.15 to impose cracking of joints within continuum volume. These combined variations reflect the iterative calibration strategy aimed at balancing stiffness, strength, and energy dissipation while improving agreement with observed damage mechanisms. Building on these model variations, the next section evaluates the influence of these variations on the global response metrics and damage mechanisms through cross-comparison.

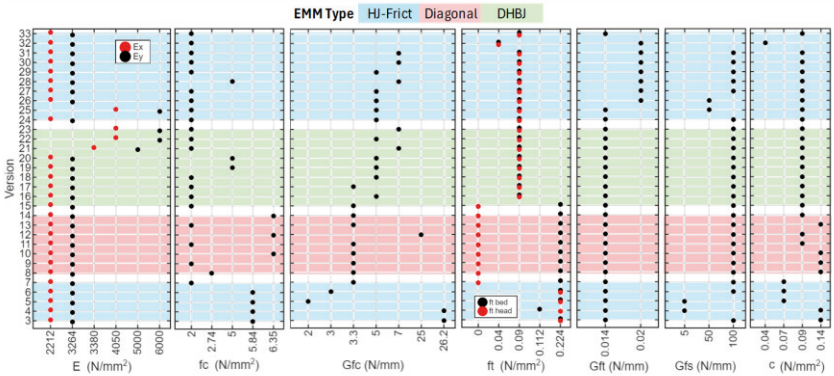

Fig. 7 Variations in material properties among the models

4.2 Cross-comparison and key takeaways

To evaluate the influence of material property variations on global structural behaviour, all force-displacement (F-D) responses obtained from monotonic pushover analyses in the positive direction were plotted together with the experimental hysteresis and backbone curve (Fig. 8a). From this set, six models, V3, V8, V9 (early models), V28 (intermediate model), V31, and V33 (advanced models), were selected for detailed cross-comparison based on F-D response (Fig. 8b), and crack pattern evolution (Fig. 8d). V3 significantly overestimated lateral strength and lacked post-peak degradation, with failure dominated by in-plane rocking and diagonal cracking. V8 introduced strength degradation but still overpredicted lateral capacity and showed limited damage redistribution between cycles. Lower energy dissipation was recorded. V9 offered a slight improvement in energy dissipation and more localised cracking, yet the global response was still misaligned with experimental trends. Among the early models, compressive strength and fracture energy in compression are the dominating parameters. V28 achieved higher energy dissipation and exhibited smeared cracking across in-plane and out-of-plane walls, including diagonal cracks consistent with experimental observations. Nevertheless, its monotonic pushover curve exceeded the experimental backbone, reflecting an acceptable strength overestimation. Under cyclic loading, alternating directions would reduce stiffness and promote higher energy dissipation, which could align with the experimental one. Excessive cracking at Cycle 15 compared to the experiment (Fig. 3) indicated overestimation of damage progression. In this case, a combination of reduced compressive strength, tensile strength and fracture energy in compression with increased fracture energy in tension plays a critical role. V31 reduced lateral strength closer to the experimental value and captured the rocking mechanism at piers and diagonal cracking in the out-of-plane walls. Despite an improved mechanism, energy dissipation remained low. To address this, V33 slightly increased compressive fracture energy while reducing tensile fracture energy, resulting in a more distributed crack pattern and enhanced energy dissipation. Cycle 15 captured propagation into the second floor, including diagonal and vertical cracks, closely matching experimental observations. Table 1 summarises the comparative performance of selected models, highlighting V33 as the version achieving a reasonable compromise between global response and mechanism. Therefore, V33 was accepted as the calibrated model. Monotonic loading resulted in concentrated cracking at critical regions, while cyclic loading caused smeared cracking distributed across the components. This behaviour is typical of the continuum modelling approach, where repeated load reversals promote gradual damage spread rather than sharp localisation. The cyclic pushover envelope closely follows the experimental backbone, indicating good global agreement (Fig. 8d). Initial stiffness is slightly lower than the experiment, likely due to idealised boundary conditions and simplified material properties. Lateral strength in both positive and negative directions is reasonably well captured. Hysteretic loops show similar trends, though unloading/reloading paths differ because the numerical protocol used one cycle per displacement target, while multiple cycles were applied in the experiment. Thus, energy dissipation is lower given the simplified cyclic load protocol and absence of localised damage modelling. Matching force-displacement curves alone was insufficient; the selection was guided by mechanism verification, including crack evolution, redistribution, and modes, to ensure consistency with experimental observations. These findings highlight the epistemic uncertainty inherent in the continuum modelling approach.

Tab. 1 Performance comparison of the models and experiment

Criterion	V3	V8	V9	V28	V31	V33
Elastic Stiffness	A	A	B	B	B	B
Base Shear at Cycle 15	C	D	C	C	B	A
Base Shear at Cycle 21	D	B	A	D	B	A
Strength Degradation	D	C	B	B	B	A
Energy Dissipation	D	D	C	C	B	C
Damage Mechanism	D	C	C	C	C	A
A: Good, B: Acceptable, C: Moderate, D: Poor						

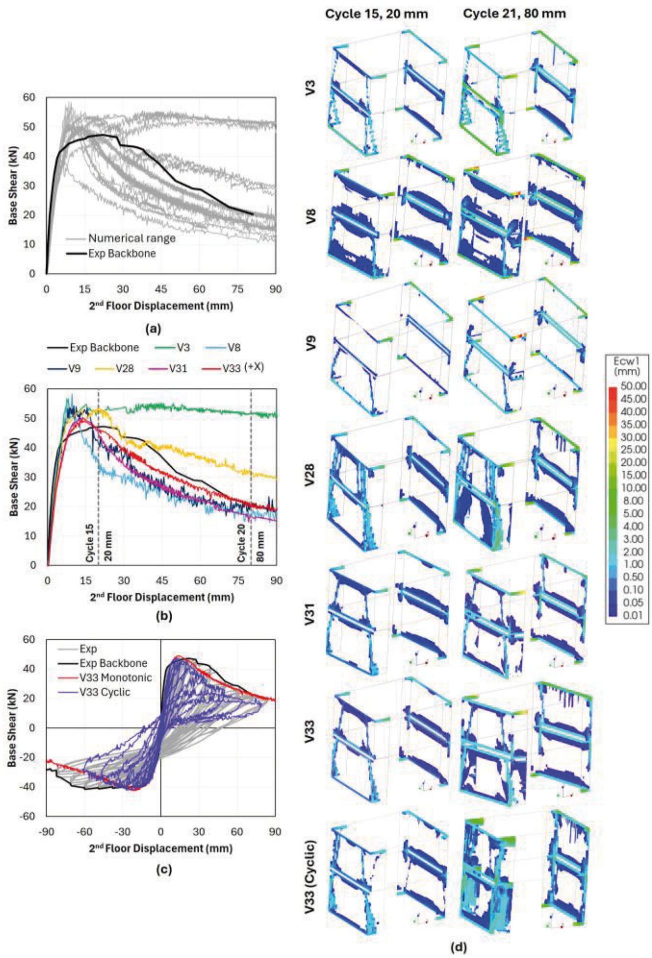

Fig. 8 Cross comparison among the variations: force-displacement response (a- b-c) and damage mechanisms (d) compare against Fig.3.

5 Conclusions

This study investigated the calibration of a continuum finite element model for a calcium silicate URM building, addressing the research gap of relying solely on global response metrics for validation. A mechanism-based evaluation is essential to ensure that numerical models replicate not only stiffness and strength but also the governing damage mechanisms and their progression observed experimentally. Compressive strength and fracture energy in compression were identified as the most influential parameters for simulating calcium silicate masonry behaviour due to brittle brick splitting. Significantly lower values of these parameters are required to reproduce the brittle post-peak response within the continuum approach. Agreement in damage mechanisms should be treated as a prerequisite for model validation rather than a posterior check. Importantly, the calibration process is subject to epistemic uncertainty, arising from modelling assumptions, parameter interdependencies, and simplifications inherent in continuum approaches. Consequently, material properties become inherently model-dependent, and this dependency must be acknowledged and accepted as part of the modelling philosophy. Rather than relying solely on material characterisation data, calibration should focus on achieving consistency between structural-level behaviour and observed mechanisms.

6 References

[1] Aşıkoğlu A, et al. Pushover analysis of unreinforced irregular masonry buildings: Lessons from different modeling approaches. Eng Struct; 2020.

[2] Parisse F, et al. Benchmarking the seismic assessment of unreinforced masonry buildings from a blind prediction test. Structures; 2021.

[3] Cattari S, Magenes G. Benchmarking the software packages to model and assess the seismic response of unreinforced masonry existing buildings through nonlinear static analyses. Springer Netherlands; 2022.

[4] Tomić I, et al. Shake-table testing of a stone masonry building aggregate: overview of blind prediction study. Bulletin of Earthquake Engineering; 2024.

[5] Ravenshorst G., et al. Structural behaviour of a calcium silicate brick masonry assemblage: Quasi-static cyclic pushover and dynamic identification test (C31B60-7). TU Delft; 2016.

[6] DIANA FEA. DIANA Finite Element Analysis (v. 10.10) 2025.

[7] Jafari S. Material characterisation of existing masonry: A strategy to determine strength, stiffness and toughness properties for structural analysis. TU Delft; 2021.

[8] Pari M, et al. Calibration of Computational Models for the Reproduction of Damage in Calcium-Silicate Brick Masonry Walls. TU Delft; 2023.